Bio-Medical Materials and Engineering 35 (2024) 415–423
DOI 10.3233/BME-230049
IOS Press
AUTHOR COPY

Design and simulation of scaffolds with lattice microstructures for bioprinting bone tissue

Esmeralda Zuñiga-Aguilar[a], Odin Ramírez-Fernández[b,c,*] and Adeodato Botello-Arredondo[c]
[a]*Department of Electrical and Computational Engineer, Instituto de Ingeniería y Tecnología, Universidad Autónoma de Ciudad Juárez, Ciudad Juárez, Mexico*
[b]*Universidad Tecnologica de Mexico (UNITEC), Ciudad de México, Mexico*
[c]*Tecnológico de Monterrey, Monterrey, Mexico*

Received 16 April 2023
Accepted 29 July 2024

Abstract.
BACKGROUND: Tissue engineering seeks to improve, maintain, or replace the biological functions of damaged organs or tissues with biological substitutes such as the development of scaffolds. In the case of bone tissue, they must have excellent mechanical properties like native bone.
OBJECTIVE: In this work, three geometric models were designed for scaffolds with different structure lattices and porosity that could be biomechanically suitable and support cell growth for trabecular bone replacement applications in tissue engineering and regenerative medicine to the proximal femur area.
METHODS: Geometries were designed using computer-aided design (CAD) software and evaluated using finite element analysis in compression tests. Three loads were considered according to the daily activity: 1177 N for slow walking, 2060 N for fast walking, and 245.25 N for a person in a bipedal position. All these loads for an adult weight of 75 kg. For each of them, three biomaterials were assigned: two polymers (poly-glycolic acid (PGA) and poly-lactic acid (PLA)) and one mineral (hydroxyapatite (HA)). 54 tests were performed: 27 for each of the tests.
RESULTS: The results showed Young's modulus (E) between 1 and 4 GPa.
CONCLUSION: If the resultant E is in the range of 0.1 to 5 GPa, the biomaterial is considered an appropriate alternative for the trabecular bone which is the main component of the proximal bone. However, for the models applied in this study, the best option is the poly-lactic acid which will allow absorbing the acting loads.

Keywords: Scaffold, lattice, femur, tissue engineering, biomechanical

1. Introduction

Tissue engineering is the application of principles and methods of engineering and life sciences to obtain a fundamental understanding of structure-function relationships in normal and pathological tissue [1]. Bone is the second most transplanted tissue in the body caused by trauma, tumors, infections, and congenital defects [2]. The tissue engineering approach involves the regeneration of new supports such as

*Corresponding author: Odin Ramírez-Fernandez, Universidad Tecnologica de Mexico (UNITEC), Mexico Campus en Linea, Av. Marina Nacional No. 162, Col. Anáhuac, Ciudad de México, CP 11320, Mexico. E-mail: odinramirezfernandez@gmail.com.

bone tissue, these require an ideal microenvironment, as well as adequate biomechanics that simulate the original site, this environment is provided by the scaffold [3].

Scaffolds are the masterpiece of bone tissue engineering. A bone scaffold is the 3D matrix that allows and stimulates the attachment and proliferation of osteoinducible cells on its surfaces. The following concerns must be considered in designing bone scaffolds: biocompatibility, biodegradability, mechanical properties to bear weight, proper porosity [4]. Some researchers consider a minimum of porosity of 50% and a range of pore size of 100–1500 μm to provide sufficient surface area for cell adhesion and to allow bone ingrowth [5–8].

An emerging strategy is the use of lattice structures to construct scaffolds [6]. According to Tang [7], lattice structures are more flexible and customizable to achieve a desired physical property. In addition, 3D printing provides an opportunity for generating structures lattices, that have properties like bone and potentially better mechanical efficiency [8].

To design the ideal scaffold, a full understanding of the compositions, structures, and biomechanical and biochemical properties of natural bone is required [9]. Bone is a natural composite with a cell-seeded mineralized collagen matrix. It is mainly composed of minerals (50–60 wt. %), collagen (30–40 wt. %), and water (10–20 wt. %) [10]. Bone is a dynamic adaptive connective tissue composed of cells and extracellular matrix. It has three main functions: structural, support, protection and locomotion, hematopoiesis, a reservoir for calcium and phosphate.

The bone tissue, from a macroscopic level, is organized in the bones in two ways: the compact or cortical bone and the trabecular or cancellous bone [11]. Bones are subjected to mechanical loads, which are determined by gravitational forces and associated muscle contractions [12]. Either constant or cyclical loading can be used for experimental strength testing, the most widely used is bending, torsional, compressive, and tensile loads [13].

Regarding mechanical characteristics, bone has been considered transversely as an isotropic material. Trabecular bone tissue is complex due to the heterogeneity it presents, an example is found at the ends of the femur, in the trabecular area, which presents anisotropy and can have a behavior like that of the cortical area, due to the orientation adopted by the trabeculae. The isotropy of the trabecular area would therefore depend on the stress acting on each area of the bone since stress determines the orientation of the trabeculae. The behavior variability of trabecular bone has given rise to different criteria when selecting the mechanical model that best represents its performance. In many studies, the problem is solved by considering bone as an isotropic material and sometimes as an orthotropic material [14].

The mechanical properties of cancellous human bone also depend on porosities in its structure because it consists of a non-uniform porous structure, the density of which gradually increases from the inner bone to the outer bone. The structures change along the bone surface according to Young's modulus, compression strength, biocompatibility and bone ingrowth, and the compressive strength of cancellous bone ranges from 2 to 12 MPa and its modulus of elasticity is in the range of 0.1–5 GPa [9].

Biomaterials are natural or synthetic substances that are in contact with biological systems and help to repair or replace any tissue of the body [15]. The choice of one material will depend on the application and the type of function that needs replacement. Unfortunately, none of the existing biomaterials can meet all of the mechanical properties [16].

For the present work, synthetic polymers were chosen as scaffolds for their excellent mechanical properties. These polymers consist of aliphatic polyesters such as polylactic acid (PLA) and polyglycolic acid (PGA), in addition to hydroxyapatite (HA) as chosen materials. These were selected for their capability to mimic bone tissue and provide a higher osteoblasts adherence and proliferation compared to other materials [4].

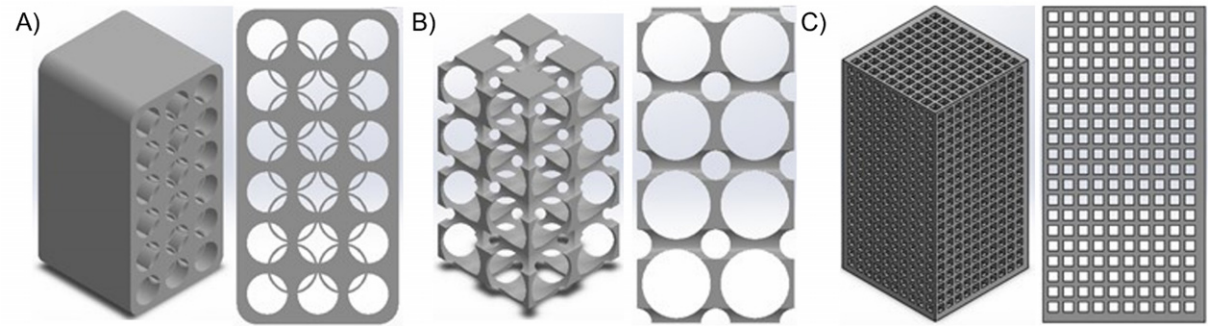

Fig. 1. Isometric and frontal view of the designed geometrical models. (A) Mandal, (B) Circles, and (C) Squared.

Table 1
Properties assigned to materials

Biomaterial	Elasticity modulus (E)	Poisson ratio
Hydroxyapatite (HA)	2 GPa	0.3
Polyglycolic acid (PGA)	4.1 GPa	0.3
Polylactic acid (PLA)	2.7 GPa	0.3

Three lattice-type scaffolds are presented in this work, shown in Fig. 1. The three models were tested and analyzed with a FEA software, in order to understand the physiology and biomechanics of trabecullar bone when subjected to mechanical loads and study their application (such as test models) in this study.

2. Materials and methods

The computational geometrical models of the cellular lattice structures were designed and generated using computer-aided design (CAD) software (SolidWorks, 2021). The dimensions (in millimeters) of the scaffolds were 16 × 16 × 3. The first geometry shown in Fig. fig1a has a porosity of 40.84%, the second model in Fig. 1b has a higher porosity structure of 88.9%, and the last model shown in Fig. 1c has a porosity of 69.3%. The mechanical properties for the three biomaterials selected (PGA, PLA and HA) are shown in Table 1. These were considered elastic linear and isotropic materials.

A mesh for each geometry was generated in the FEA software (ANSYS, 2019) prior to the mechanical analysis. Tetrahedral elements were used resulting in the following number of elements in each computational model: 20,718 elements for the mandala design (model A), 16,216 for the circles pattern (model B), and finally 94,469 elements for the squared pattern (model C), as shown in Fig. 2.

The models were evaluated under three case scenarios with equivalent loads representing an activity: for a slow-walking F_1 = 1177 N, for a fast-walking F_2 = 2060 N, and a person standing 245.25 N in this position the load is the third part of the bodyweight total. This is all for a person with 75 kg of weight. The inferior face of the model was set as a fixed constraint for better stability. For the compression test, the load was applied over the opposite face of the geometry in a negative direction in the *Y* axis.

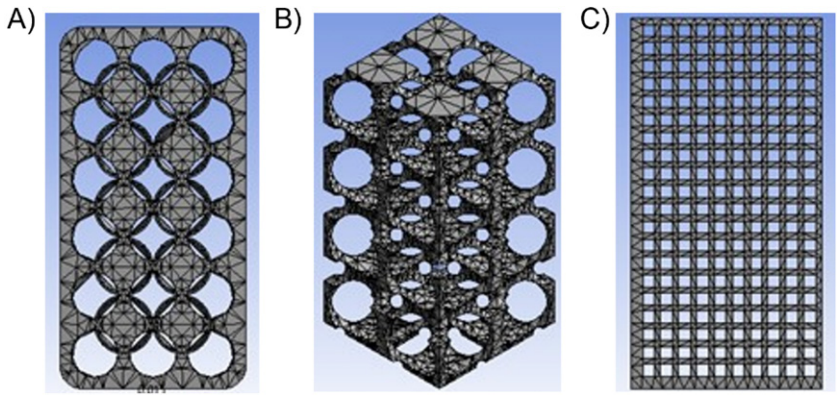

Fig. 2. Mesh generated for the geometrical models. (A) Mandal, (B) Circles, and (C) Squared.

As a result, equivalent stress and equivalent strain were requested in the postprocessing stage of the simulation. According to the strength of materials, the equivalent stress (σ_{equ}) was calculated by Von Mises criterion, and can be calculated from the stress components described by the three stress tensors or from the principal stresses in the analysis:

$$\sigma_{equ} = \sqrt{\frac{(\sigma_1 - \sigma_2)^2 + (\sigma_2 - \sigma_3)^2 + (\sigma_3 - \sigma_1)^2}{2}}.$$

Moreover, the equivalent strain (ϵ_{equ}) was calculated according to Von Mises criterion, where ν is the Poisson ratio:

$$\epsilon_{equ} = \frac{1}{1+\nu}\sqrt{\frac{(\epsilon_1 - \epsilon_2)^2 + (\epsilon_2 - \epsilon_3)^2 + (\epsilon_3 - \epsilon_1)^2}{2}}.$$

From those equations, to calculate the Modulus of elasticity for each case study, the following equation was used:

$$E = \frac{\sigma_{equ}}{\epsilon_{equ}}.$$

3. Results

Three geometries were analyzed each with three different biomaterials and three loads. Equivalent elastic stress and strain were obtained and evaluated. Figures 3 and 4 and Tables 2–4 show the values obtained after the static analysis. A stress-strain curve was drawn for each model analyzed, of which the results are shown in Fig. 5.

4. Discussion

We considered a minimum porosity of 50% in two models as biological constraints to allow bone ingrowth like it shows in Fig. 1 [17]. For the biomechanical structural analysis of scaffolds, the results

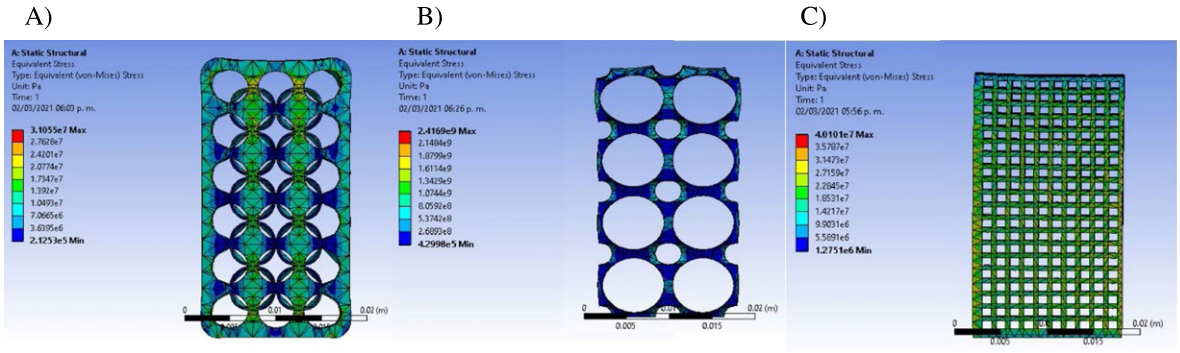

Fig. 3. Resultant equivalent elastic stress in the models with HA with a load of 1177 N. (A) Mandal, (B) Circles, and (C) Squared.

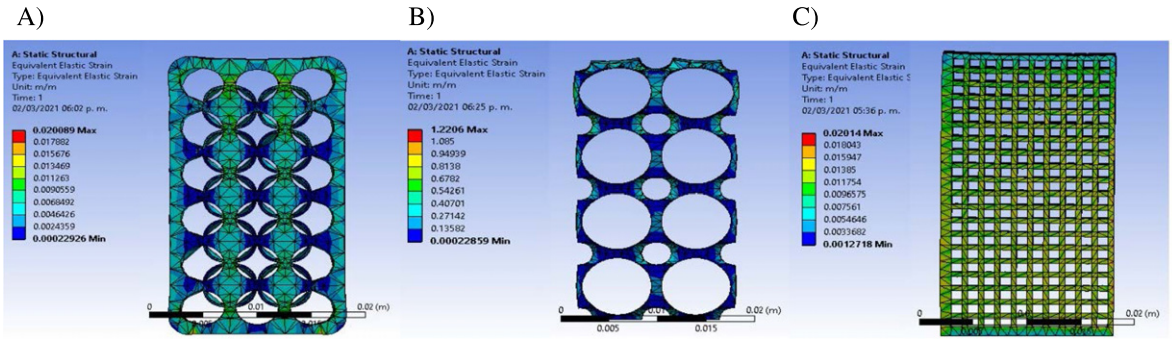

Fig. 4. Resultant strain for the models with HA with a load of 1177N. (A) Mandal, (B) Circles, and (C) Squared.

Table 2
Results in compression test for a load of 1177 N

Model	Biomaterial	Load	Equivalent elastic stress (MPa)	Strain (m/m)	Modulus of elasticity (GPa)
(A)	HA	1177 N	31.055	0.020089	1.54
(A)	PLA	1177 N	31.055	0.014881	2.08
(A)	PGA	1177 N	31.055	0.0097996	3.16
(B)	HA	1177 N	2416.9	1.2206	1.98
(B)	PLA	1177 N	2416.9	0.90414	2.67
(B)	PGA	1177 N	2416.9	0.59541	4.05
(C)	HA	1177 N	40.101	0.02014	1.99
(C)	PLA	1177 N	40.101	0.014918	2.68
(C)	PGA	1177 N	40.101	0.0098242	4.08

for equivalent stress and strain, Figs 3 and 4, were analyzed. According to the boundary and loading conditions applied on top surface, the values of equivalent stress change from top to bottom, where higher stress values are observed mainly at the first row of geometrical elements for the Mandal model, nevertheless, a distribution of stress is seen vertically; on the other hand, for the model with Circles the

Table 3
Results in compression test for a load of 2060 N

Model	Biomaterial	Load	Equivalent elastic stress (MPa)	Strain (m/m)	Modulus of elasticity (GPa)
(A)	HA	2060 N	54.35	0.03516	1.54
(A)	PLA	2060 N	54.35	0.026045	2.08
(A)	PGA	2060 N	54.35	0.017151	3.16
(B)	HA	2060 N	4230.1	2.1363	1.98
(B)	PLA	2060 N	4230.1	1.5824	2.67
(B)	PGA	2060 N	4230.1	1.0421	4.05
(C)	HA	2060 N	70.185	0.035248	1.99
(C)	PLA	2060 N	70.185	0.02611	2.68
(C)	PGA	2060 N	70.185	0.017194	4.08

Table 4
Results in compression test for a load of 245.25 N

Model	Biomaterial	Load	Equivalent elastic stress (MPa)	Strain (m/m)	Modulus of elasticity (GPa)
(A)	HA	245.25 N	6.471	0.0041859	1.54
(A)	PLA	245.25 N	6.471	0.0031007	2.08
(A)	PGA	245.25 N	6.471	0.0020419	3.16
(B)	HA	245.25 N	503.61	0.25433	1.98
(B)	PLA	245.25 N	503.61	0.18839	2.67
(B)	PGA	245.25 N	503.61	0.12406	4.05
(C)	HA	245.25 N	8.3558	0.0041965	1.99
(C)	PLA	245.25 N	8.3558	0.0031085	2.68
(C)	PGA	245.25 N	8.3558	0.002047	4.08

stress is mainly observable at small areas around the characteristic circles of the model. Moreover, the Squared model showed higher distribution of stress throughout the whole geometry.

From the stress-strain curve we can obtain a great quantity of information on the properties of the material (maximum stress, maximum strain, Young's modulus and toughness). It is possible to distinguish between a first area in which the stress and the strain are proportional and another area in which the original shape of the body does not recover [19]. In Fig. 5, Hooke's law is fulfilled according to which the deformation is proportional to the load. This part of the curve is called the "elastic region" [21]. According to the results, PLA is more suitable for the manufacture of scaffolds in bone tissue engineering due to its mechanical properties [20].

According to the calculations presented, the calculated Young's modulus is between a range of 1.54 and 4.08 GPa, similar to the range explained by previous studies [22–24], which mention that Young's modulus in human cancellous bone ranges between 0.1 and 5 GPa. These results also resemble the result of the work of Karuppudaiyan and collaborators, where they used a compressive load of 3000 N in their HA model and obtained an elastic modulus of 1.91 GPa [25]. Similarly, Dumas et al. compared their results in FEA and experimentally obtained a Young's modulus of 2.7 and 1.66 GPa correspondingly, which

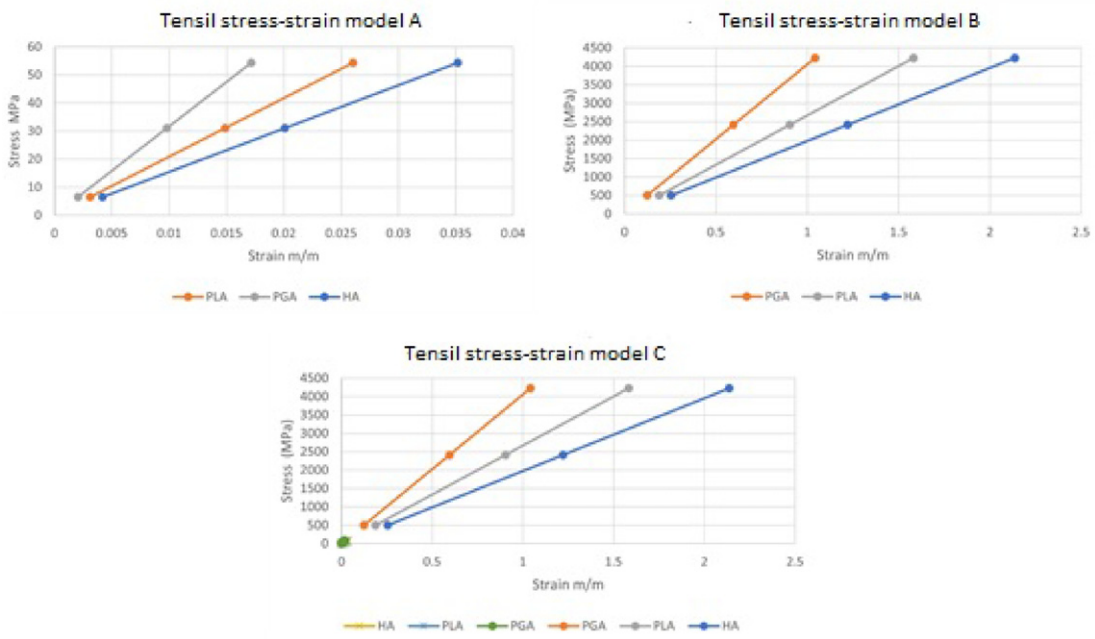

Fig. 5. Tensil stress-strain curve of models, (A) Mandal, (B) Circles, and (C) Squared.

resembles the results obtained in the Mandal model whose assigned material was PLA [17]. Finally, the highest value of stiffness was close to the higher limit of the Young's modulus in the cancellous bone [23]. Therefore, flexible materials improve the load transmission thus a better stress distribution [26].

5. Conclusions

The present work had the objective of designing and manufacturing lattice microstructures for bone scaffolds. The mechanical simulation through natural compression shows close values to those calculated on a person's walk. After analyzing the three proposed models of lattice geometries using ANSYS, it was shown that in both tensile and compression tests, the modulus of elasticity was identical in the three models whose material used was PGA, PLA and HA without presenting modifications in the three different loads used for the previously mentioned conditions. This is because for linear and isotropic elastic materials, Young's modulus is the same for tension and compression as mentioned by Torres et al. [27]. In the models whose assigned material was PGA, a higher Young's modulus was obtained, and in those assigned with HA, a lower Young's modulus was obtained. However, it was not possible to determine the elastic limit and the maximum resistance by the graphs. A greater Von Mises stress was obtained in the Mandal model. This demonstrates that if we apply more loads, we can calculate the elastic limit or the point of maximum resistance. These indicators are superior to other structures making it the most resistant model. More studies on this are necessary in the future.

The Von Mises stress criterion is particularly useful for predicting yielding of materials under complex loading conditions. It combines the three principal stresses into a single scalar value, which is crucial when dealing with complex, multi-axial stress states typical in biomaterials designs. The scaffold and structural components experience various stress combinations, making it essential to use a stress measure

that accounts for this complexity. Finally, according to the resulting calculations, Young's modulus values range between 1.54 and 4.08 GPa. In the models with PGA, the Young's modulus had higher values than those calculated for HA.

It is important to mention that one of the main problems in scaffold manufacturing for bone, is the low mechanical strength, and it is highly important to manufacture and test scaffolds with appropriate mechanical properties to those of natural and healthy bone [28]. A fundamental aspect appointed in this study, the calculated Young's modulus is shown to be in the range of 0.1 to 5 GPa, the range value for natural trabecular bone in the proximal femur, the zone on which this work is focused. Therefore, the three proposed models could follow up an experimental study with 3D bioprinted models to validate the computational work presented in this study. Moreover, the three models could potentially be good options for further in-vitro studies by using the 3D bioprinted models applied to the proximal zone of the human femur. This opens up the possibility of using these scaffolds as temporary support systems with a porous internal architecture that mimics the internal structure of the bone as closely as possible, thus promoting the growth of native tissue on top of it and achieving osseointegration of the material helps repair tissue where needed.

Conflict of interest

The authors declare that they have no conflicts of interest to report regarding the present study.

Funding

The authors received no specific funding for this study.

References

[1] Q. Chen, C. Zhu and Thouas G.A, Progress and challenges in biomaterials used for bone tissue engineering: Bioactive glasses and elastomeric composites, *Prog. Biomater.* **1** (2012), 1–16. doi:10.1186/2194-0517-1-2.
[2] M. Kheirallah and H. Almeshaly, Bone graft substitutes for bone defect regeneration. A collective review, *Int. J. Dent. Oral Sci.* **4** (2016), 247–255. doi:10.19070/2377-8075-1600051.
[3] D. Gaviria-Arias and L. Caballero-Méndez, Fibroin from silkworm (Bombyx mori L) as biomaterial used in regenrative medicine process based on tissue engineering, *Med. Regen. basada en Ing. tejidos*. **21** (2015), 38–47. doi:10.22517/25395203.9411.
[4] T. Ghassemi, A. Shahroodi, M.H. Ebrahimzadeh, A. Mousavian, J. Movaffagh and A. Moradi, Current concepts in scaffolding for bone tissue engineering, *Arch. Bone Jt. Surg.* **6**(2) (2018), 90–99. doi:10.22038/abjs.2018.26340.1713.
[5] C. Yan, L. Hao, A. Hussein and P. Young, Ti-6Al-4V triply periodic minimal surface structures for bone implants fabricated via selective laser melting, *J. Mech. Behav. Biomed. Mater.* **51** (2015), 61–73. doi:10.1016/j.jmbbm.2015.06.024.
[6] P.F. Egan, V.C. Gonella, M. Engensperger, S.J. Ferguson and K. Shea, Computationally designed lattices with tuned properties for tissue engineering using 3D printing, *PLoS One* **12**(8) (2017), 1–21. doi:10.1371/journal.pone.0182902.
[7] Y. Tang, G. Dong and Y.F. Zhao, A hybrid geometric modeling method for lattice structures fabricated by additive manufacturing, *Int. J. Adv. Manuf. Technol.* **102**(9–12) (2019), 4011–4030. doi:10.1007/s00170-019-03308-x.
[8] P.F. Egan, K.A. Shea and S.J. Ferguson, Simulated tissue growth for 3D printed scaffolds, *Biomech. Model. Mechanobiol.* **17**(5) (2018), 1481–1495. doi:10.1007/s10237-018-1040-9.
[9] S. Wu, X. Liu, K.W.K. Yeung, C. Liu and X. Yang, Biomimetic porous scaffolds for bone tissue engineering, *Mater. Sci. Eng. R Reports* **80**(1) (2014), 1–36. doi:10.1016/j.mser.2014.04.001.
[10] M.J. Mirzaali et al., Mechanical properties of cortical bone and their relationships with age, gender, composition and microindentation properties in the elderly, *Bone* **93** (2016), 196–211. doi:10.1016/j.bone.2015.11.018.
[11] J.D. Black and B.J. Tadros, Bone structure: From cortical to calcium, *Orthop. Trauma* **34**(3) (2020), 113–119. doi:10.1016/j.mporth.2020.03.002.

[12] M. Corina, V. José, L. Ferretti, V. Abdala and G.R. Cointry, Biomechanical properties of anuran long bones: Correlations with locomotor modes and habitat use, *Journal of Anatomy* (2020), 1–14. doi:10.1111/joa.13161.
[13] H. Beaupied, E. Lespessailles and C.L. Benhamou, Evaluation of macrostructural bone biomechanics, *Jt. Bone Spine* **74**(3) (2007), 233–239. doi:10.1016/j.jbspin.2007.01.019.
[14] M.Á. Flores Rentería, M. Ortiz Domínguez, A. Cruz Avilés and F. López Sánchez, The mechanics of the bonE. A review of bone remodeling models, *Ingenio y Concienc. Boletín Científico la Esc. Super. Ciudad Sahagún.* **5**(9) (2018). doi:10.29057/ess.v5i9.2902.
[15] K. Tappa and U. Jammalamadaka, Novel biomaterials used in medical 3D printing techniques, *J. Funct. Biomater.* **9**(1) (2018). doi:10.3390/jfb9010017.
[16] F. Barrère, T.A. Mahmood, K. de Groot and C.A. van Blitterswijk, Advanced biomaterials for skeletal tissue regeneration: Instructive and smart functions, *Mater. Sci. Eng. R Reports* **59**(1–6) (2008), 38–71. doi:10.1016/j.mser.2007.12.001.
[17] M. Dumas, P. Terriault and V. Brailovski, Modelling and characterization of a porosity graded lattice structure for additively manufactured biomaterials, *Mater. Des.* **121** (2017), 383–392. doi:10.1016/j.matdes.2017.02.021.
[18] M. Zhou, J. Hou, G. Zhang and C. Luo, Tuning the mechanics of 3D-printed scaffolds by crystal lattice-like structural design for breast tissue engineering, *Geophys. Res. Lett.* (2020), 0–31. doi:10.1088/1758-5090/ab52ea. .
[19] J.R. Caeiro, P. González and D. Guede, Biomechanics and bone (& II): Trials in different hierarchical levels of bone and alternative tools for the determination of bone strength, *Rev. Osteoporos. y Metab. Miner.* **5**(2) (2013), 99–108.
[20] A. Bagheri, I. Buj-Corral, M. Ferrer, M.M. Pastor and F. Roure, Determination of the elasticity modulus of 3D printed octet-truss structures for use in porous prosthesis implants, *Materials (Basel).* **11**(12) (2018). doi:10.3390/ma11122420.
[21] M.S. Nazir et al., Analysis of the biomechanical behavior of the femoral epiphysis in 6-year-old children affected by avascular necrosis: Computational model, *Spectrochim. Acta - Part A Mol. Biomol. Spectrosc.* **192**(4) (2018), 121–130.
[22] S.P. Singh, T. Bhardwaj and M. Shukla, Lattice modeling and finite element simulation for additive manufacturing of porous scaffolds, in: *2017 Int. Conf. Adv. Mech. Ind. Autom. Manag. Syst. AMIAMS 2017 - Proc.*, 2017, pp. 333–336. doi:10.1109/AMIAMS.2017.8069234.
[23] P. Feng, P. Wei, C. Shuai and S. Peng, Characterization of mechanical and biological properties of 3-D scaffolds reinforced with zinc oxide for bone tissue engineering, *PLoS One* **9**(1) (2014). doi:10.1371/journal.pone.0087755.
[24] M.-P. Alberto and M.-P. Laura, Matrices para Ingenieria del tejido Oseo, *Actual. Medica* (2019), 36–45. doi:10.15568/am.2019.806.re.01.
[25] S. Karuppudaiyan, D. Kingsly Jeba Singh and V.M. Santosh, Finite element analysis of scaffold for large defect in femur bone, *IOP Conf. Ser. Mater. Sci. Eng.* **402**(1) (2018). doi:10.1088/1757-899X/402/1/012096.
[26] J.E. Gubaua, G.W.O. Dicati and J.T. Pereira, Influence of material stiffness of total hip prosthesis in isotropic bone-remodeling process analysis, in: *Proc. XXXVIII Iber. Lat. Am. Congr. Comput. Methods Eng.*, 2017. doi:10.20906/cps/cilamce2017-0211.
[27] G. Torres, B. Tutor and L.I. Negr, Aplicación de la extensometría eléctrica y la simulación computacional en la realización del ensayo de tracción. 2018.
[28] M. Rahatuzzaman, M. Mahmud, S. Rahman and M.E. Hoque, Design, fabrication, and characterization of 3D-printed ABS and PLA scaffolds potentially for tissue engineering, *Results Eng.* **21** (2024), 101685. doi:10.1016/j.rineng.2023.101685.